JOURNAL OF APPLIED PHYSICS VOLUME 93, NUMBER 8 15 APRIL 2003

Competition between ferroelectric and semiconductor properties in $Pb(Zr_{0.65}Ti_{0.35})O_3$ thin films deposited by sol–gel

I. Boerasu[a)]
Centro de Fisica, Universidade do Minho, Campus de Gualtar, 4710-057 Braga, Portugal

L. Pintilie
National Institute for Materials Physics, Bucharest-Magurele, P.O. Box MG-7, Romania

M. Pereira, M. I. Vasilevskiy, and M. J. M. Gomes
Centro de Fisica, Universidade do Minho, Campus de Gualtar, 4710-057 Braga, Portugal

(Received 21 October 2002; accepted 27 January 2003)

Asymmetric metal–ferroelectric–metal (MFM) structures were manufactured by sol–gel deposition of a lead zirconate-titanate (PZT with Zr/Ti ratio 65/35) film on Pt-coated Si, with a Au top electrode. The average remnant polarization of 9 $\mu C/cm^2$ and the coercive field of 39 kV/cm were obtained from the hysteresis loop measurements. A detailed analysis of the polarization–electric field ($P-E$), capacitance–voltage ($C-V$), and current–voltage ($I-V$) measurement results allowed us to estimate the near-electrode space-charge region thickness (roughly half of the film thickness at zero voltage), net doping concentration (around 10^{18} cm^{-3}), built-in potential (in the 0.4–0.8 V range, depending on the injecting electrode), and dynamic dielectric constant (5.2). The current logarithm–voltage dependence for the field-enhanced Schottky emission obeys a ''1/4'' law. The spectral distribution of the short circuit current measured under continuous light illumination in the 290–800 nm range exhibits a cutoff wavelength at 370 nm and a maximum sensitivity at about 340 nm. The estimated band-gap energy of the PZT material is 3.35 eV. The MFM structure is discussed in terms of two back-to-back Schottky diodes with a ferroelectric material in between. It is concluded that the semiconductor properties of the films are not negligible and, in certain conditions, are dominating over the ferroelectric ones. © *2003 American Institute of Physics.* [DOI: 10.1063/1.1562009]

I. INTRODUCTION

Ferroelectric thin films, especially of lead titanate-zirconate [$Pb(Zr_xTi_{1-x})O_3$] solid solutions (known as PZT), have been of great interest in the last decade for their applications in electronic devices, such as nonvolatile memories, infrared sensors, optical shutters, modulators, etc.[1–3] A variety of techniques has been proposed to fabricate PZT films, such as metallorganic chemical vapor deposition (MOCVD), sputtering, sol–gel, and pulsed laser ablation (PLD). Among them, the sol–gel method is the most popular because of its low cost and easy application to the PZT system.[4] The method is well developed and can be used to prepare good perovskite films at low temperatures. A large number of studies have been dedicated to the investigation of the structural, electric, ferroelectric and photoelectric properties of PZT thin films.[5–8] Depending on the target application of the film, the interest was focused on one property or another. For example, in the case of films for memory applications, the interest was focused on polarization retention, imprint, and fatigue, with the aim to elucidate the mechanisms involved in these phenomena.[9] Internal electric fields developed by charged defects near the electrodes or in the film volume are believed to play an important role in these phenomena.[10,11] Thus, correlated polarization–electric field ($P-E$), capacitance–voltage ($C-V$), and current–voltage ($I-V$) measurements are necessary in order to reveal the presence of space-charge regions (SCR) and to elucidate the problem of conduction mechanisms in PZT thin films.

It seems likely that the semiconductor character of PZT could be no longer neglected in such applications. The band gap of PZT-type materials is rather large, around 3.2–3.7 eV.[12–14] However, the inevitable presence of defects acting as doping centres makes its semiconductor properties important for the electrical and optical processes in PZT-based structures. The interplay between the ferroelectric and semiconductor properties seems to be crucial for deciding if a PZT film is good for a certain application or not. In the case of memory applications, the requirements include high remnant polarization, low coercive field allowing operation at low voltages, good square hysteresis loop, short switching times, good retention, and fatigue properties. They correspond to a material with very good ferroelectric properties. On the other hand, large leakage current, large concentration of defects acting as trapping centers and the presence of Schottky barriers at contacts are more characteristic to a semiconductor material. These properties can interfere with ferroelectric ones making the film useless for memory applications. The same is valid for other applications, for example, for light detection. If the film has good polarization properties, low dielectric constant, and high pyroelectric coefficient, it could be useful for pyroelectric detection in the

a)Electronic mail: iulian@fisica.uminho.pt

infrared (IR) domain of the spectrum.[15,16] If the film exhibits good photoconductivity or photovoltaic effect (almost inherent in the presence of internal electric fields), it could be useful as detector material for the ultraviolet (UV) spectral region.[17] Therefore, both the semiconductor and ferroelectric properties of PZT films should be thoroughly investigated prior to deciding what type of application the studied material is good for.

In this article, we report on the electric, ferroelectric, and photoelectric properties of sol–gel-grown PZT films with 65/35 value of Zr/Ti ratio. This composition lies in the rhombohedral part of the $PbZrO_3-PbTiO_3$ system phase diagram and has been less studied than those near the morphotropic phase boundary. We analyze our experimental results in terms of existing models for ferroelectric[18] and semiconductor[19] materials. It will be shown that the semiconductor or ferroelectric properties are dominant depending on whether the electric field applied to the sample is continuous (dc) or alternating (ac).

II. EXPERIMENTAL DETAILS

The PZT thin films were prepared using lead acetate, zirconium-tetra *n*-butoxide and titanium-tetra-isopropoxide as precursors. 2-metoxyethanol was used as solvent. The molar ratio of Zr/Ti was 65/35 and a 5% excess of the lead precursor was added to the solution to compensate the deficiency in lead concentration and to assist the crystallization. $Si/SiO_2/TiO_2/Pt$ wafers were used as substrates. The crystallization was performed by conventional thermal annealing at 650 °C, for 60 min in air. More details about the deposition process are given in Ref. 12. The final metal/ferroelectric/metal (MFM) structure was obtained by evaporation of semitransparent gold top electrode (250 μm in diameter) using a shadow mask. Note that the structure is asymmetric in terms of electrodes, the bottom one is platinum and the top electrode is gold. An interfacial layer could form at the interface with Pt electrode during crystallization annealing, altering the properties of the PZT film.[20,21]

The crystalline structure of the PZT film was analyzed by x-ray diffraction (XRD) using Cu $K\alpha$ radiation. The $I-V$ characteristics were recorded using a computer controlled Keithley 617 electrometer with a 100 V dc built-in voltage source. Prior to the $I-V$ measurement the film was poled by applying a voltage of ± 5 V for several minutes. During the $I-V$ measurements the voltage was varied in steps of 50 mV, with a delay time of 30 s before current readings. Almost steady-state currents were measured this way, with no significant difference between two orientations of ferroelectric polarization. The polarity of the applied voltage was considered with respect of the gold (top) electrode. The $C-V$ measurements were performed using a HP 4284A *LCR* bridge, at 100 kHz and with a 0.2 V amplitude ac signal. The $P-E$ curves were measured at 100 kHz using a modified Sawyer–Tower circuit. Finally, the photoelectric measurements were performed using a computer-controlled setup consisting of a grating monochromator Spex 270M and a 500 W Xe arc lamp as light source. The generated photocurrent was measured with the Keithley 617 electrometer.

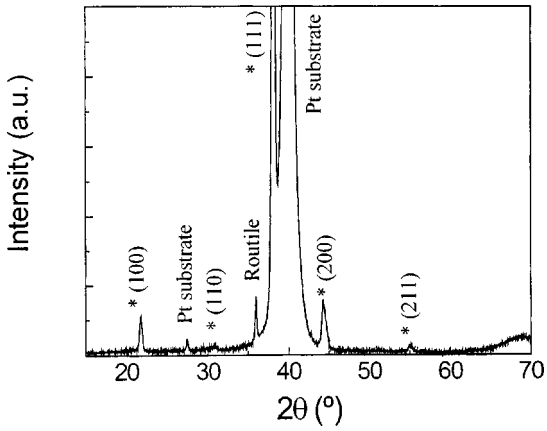

FIG. 1. XRD pattern of a ferroelectric PZT 65/35 thin film deposited by sol–gel. The asterix indicates characteristic peaks of perovskite phase.

III. RESULTS

A. Structural and morphological properties

The x-ray diffraction spectrum (Fig. 1) of as-deposited films presents intense peaks of the perovskite rhombohedral phase, with preferred orientation in the (111) direction. This conclusion was deducted analyzing the peak intensities. The preferential growth in the (111) direction is due to the platinum substrate, as was suggested in literature.[21] The x-ray analysis also proves the absence of secondary phases such as pyrochlore. This conclusion is supported by the fact that the only peaks occurring in the spectrum correspond to rhombohedral perovskite phase, to the platinum substrate, and to the routil (TiO_2) layer. The last one was deposited on top of the SiO_2/Si substrate in order to increase the platinum adherence.

B. Ferroelectric and electrical properties

A typical $P-E$ hysteresis loop of one of our films is shown in Fig. 2. This curve was obtained by processing the recorded experimental data and taking into account that the charge collected from the reference capacitor in the Sawyer–Tower setup is, in fact, proportional to the electric displacement D, according to the following equation:

$$D=\varepsilon_0\varepsilon_r E+P_S, \tag{1}$$

where P_S is the spontaneous polarization, E the applied electric field, and ε_r the dielectric constant of the ferroelectric film. This quantity derives from the linear part of polarization response to applied electric field. It can be determined from capacitance measurements performed either on fresh samples (not subjected to a poling procedure) at zero dc electric field (and using a low amplitude ac test field), or after saturating the spontaneous polarization. In the latter case, the polarization increases linearly with a further increase of the applied electric field.[22] The static dielectric constant ε_r is around 475 in our films. The value of the electric displacement was obtained by dividing the recorded scope voltage (V) by the sample electrode area (A) and multiplying by the reference capacitance C_0 (i.e., $D=VC_0/A$). Then P_S was extracted according to Eq. (1).

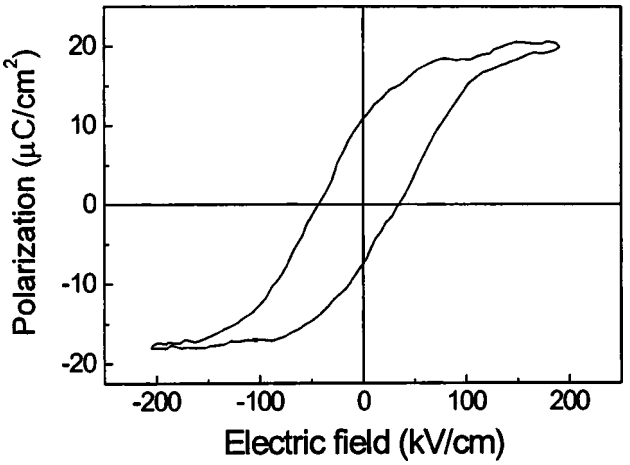

FIG. 2. Polarization vs electric field hysteresis loop of a Au/PZT(65/35)/Pt capacitor structure. The important values for remnant polarization and coercive field are: $P_r^+ = 10.8\ \mu C/cm^2$; $P_r^- = 7.4\ \mu C/cm^2$; $E_c^+ = 35$ kV/cm; and $E_c^- = 43$ kV/cm. The average values are: $P_r = 9.2\ \mu C/cm^2$ and $E_c = 39$ kV/cm.

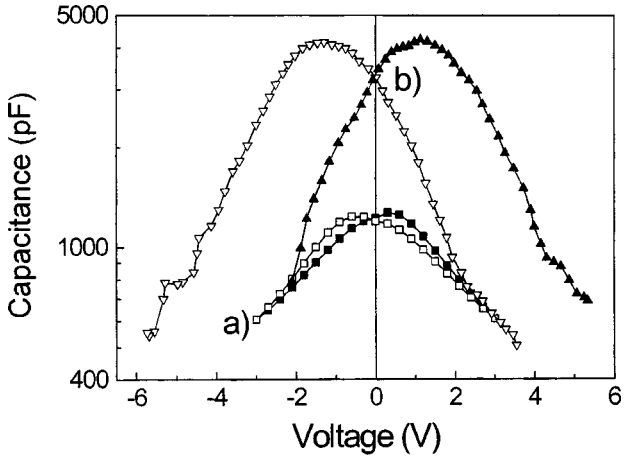

FIG. 3. $C-V$ curves for Au/PZT(65/35)/Pt capacitor: (a) with squares, as resulted from $C-V$ measurements (open squares, the applied voltage was swiped down; solid squares, the applied voltage was swiped up). (b) With triangles, as derived from $D-E$ measurements using Eq. (2) (open triangles, the applied voltage was swiped down; solid triangles, the applied voltage was swiped up).

For the hysteresis loop of Fig. 2, the average remnant polarization P_r is about 9 $\mu C/cm^2$ and the average coercive field E_c is approximately 39 kV/cm. The latter is quite a low value for PZT films. As it can be seen from Fig. 2, the hysteresis curve is asymmetric both along the field and polarization axes. The negative coercive field is slightly higher than the positive one, which suggests the presence of some internal bias due to different electrode interfaces (different work functions, probably different densities of interface states acting as traps).[23] In addition, the positive value of P_r is larger than the negative one. The polarization shift was reported in the so-called ''graded ferroelectrics''[24] but in our case of homogeneous film this shift could be related also to the electrode asymmetry.[25]

The $C-V$ curve of the same film is presented in Fig. 3, curve (a). It has a typical ''butterfly'' shape, with two maxima, which should correspond to the coercive field values.[26] Thus, if the voltage difference between the maxima is divided by the film thickness, then roughly twice the value of the coercive field should be obtained. This gives a coercive field of about 18.5 kV/cm, which is much lower than that obtained from the $P-E$ curve. At this point, it is worth noting that the $C-V$ curve is measured applying a dc bias (the ac testing signal is small), which means that space-charge regions may develop near the contacts and follow the bias even if the kinetics of this process is slow. If this happens, the internal electric field present in SCR can impede the polarization reversal. Thus, the film thickness acting as a real ferroelectric should be considerably reduced. We will return to this point in the next section.

The capacitance variation with changing the applied voltage can also be obtained by deriving the $D-E$ (dielectric displacement versus electric field) curve,

$$C_{D-E} \equiv \frac{dQ_D}{dV} = \frac{dQ_P}{dV} + C_0. \tag{2}$$

In Eq. (2), $Q_D = DA$, $Q_P = P_S A$, $C_0 = \varepsilon_0 \varepsilon_r A/d$, A is the contact area, and d the total thickness of the ferroelectric film. It has been assumed that the film is uniform and $E = V/d$. The capacitance calculated using Eq. (2) is presented in Fig. 3, curve (b). It can be seen from Fig. 3 that C_{D-E} is much larger than the directly measured capacitance. Again, this fact can be understood if we assume that there are SCRs near the metallic contacts, which considerably shrink the part of the film behaving as a normal ferroelectric, in which polarization reversal is possible.

The presence of the SCR in the MFM structures lead us to the idea of considering these structures as two back-to-back Schottky contacts, with a ferroelectric layer between them. For sufficiently high (positive or negative) voltages the $C-V$ curves should be similar to those of a Schottky diode. The latter is described by the following relation:[19]

$$\frac{1}{C^2} = \frac{2}{A^2 q N_A \varepsilon_0 \varepsilon_r}\left(V + V_{\text{bi}} - \frac{kT}{q}\right), \tag{3}$$

where C is the measured capacitance; V_{bi} the built-in voltage and N_A the acceptor concentration, or more accurate, net space-charge concentration; k is Boltzma's constant; T is temperature; and q is elementary charge. The kT/q term is usually neglected compared to $V + V_{\text{bi}}$. The $1/C^2$ vs V plots for the capacitance measured in $C-V$ experiments are represented in Fig. 4, from which the net doping concentration can be calculated and, from the intercept on the voltage axis, a rough estimation of the built-in potential can be made. The values obtained for the effective doping and built-in voltage V_{bi} at room temperature are given in Table I. We emphasize here that these are only rough estimations. The different values obtained for up and down voltage sweeping are due to the polarization hysteresis and asymmetric electrodes.

C. Current–voltage characteristics

During the $I-V$ measurements, the voltage polarity was defined with respect to the top electrode A representative current-voltage curve is shown in Fig. 5 (in logarithmic

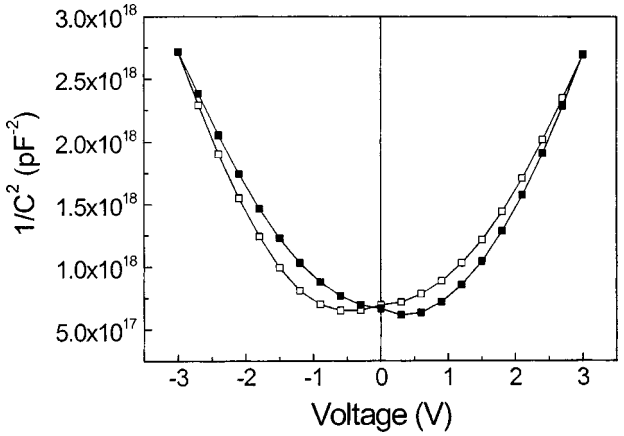

FIG. 4. $1/C^2$ vs V plot of the $C-V$ curve of Fig. 3(a) Open markers, voltage sweep down. Solid markers, voltage sweep up.

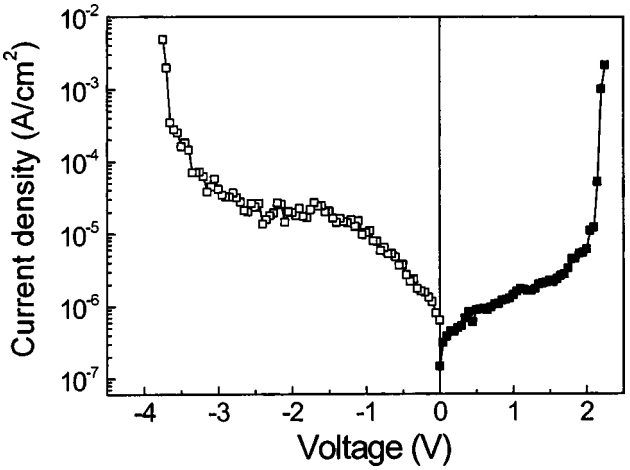

FIG. 5. Current–voltage characteristics of an Au/PZT(65/35)/Pt MFM structure.

scale). It is not symmetric, due to the electrode asymmetry, and is similar to those reported in the literature[27] for MFM structures.

D. Photoelectric characterization

The spectral dependence of the photoconductivity (PC) was studied for several values of applied voltage by illuminating through the top electrode. The measured signal (photocurrent) was normalized to the spectral distribution of the lamp. The latter one was obtained using a photomultiplier, thus the normalized curves are given in arbitrary units and are shown in Fig. 6. They display a sensitivity maximum at approximately 340 nm for all the values of applied voltage. Similar spectral distributions have been reported for PZT-type materials.[28] These results are presented and discussed in the end of the next section.

IV. DISCUSSION

A. Ferroelectric and electrical properties

The directly measured value of the capacitance of the structure, C_{C-V}, is much lower than that obtained from the hysteresis loop through Eq. (2). For instance, at $P_S=0$ and $E=E_C$ (where the maximum of the $C-V$ curve occurs) $C_{C-V}=1.21$ nF and $C_{D-E}=4.2$ nF. As mentioned in the previous section, this can be understood by admitting the existence of a SCR near at least one of the contacts, depending on the polarity of applied bias. The following discussion is based on the assumption that the PZT film is p type and behaves like a normal semiconductor.[29] If the work function of the metal electrode it is slightly larger than that of PZT (which is the case of platinum) one may expect an accumulation of holes at the interface. However, the presence of surface/interface states acting as trapping centers can induce a depletion region near electrodes.[30,31] It is assumed that such depleted regions are present at both electrode interfaces (see Fig. 7). When a voltage is applied on the structure the depletion region width will increase near the reverse biased electrode and will decrease near the other one, eventually passing to accumulation. Roughly speaking, one Schottky contact will be reverse-biased while the other one will be forward biased. However, the capacitance obtained from $C-V$ measurements is determined by the SCR capacitance (at the reverse biased interface) in series with that of the rest of the film still behaving like a ferroelectric. In the case of $D-E$ measurements, the SCR cannot follow the variation of the ac-applied field because of the low mobility of holes in perovskites[18] and large emission time constants for active traps at room temperature, so the depletion SCR may not form at all. In such a situation, we assume that the MFM structure acts as a single capacitor filled with the ferroelectric material [see Eq. (2)].

TABLE I. Acceptor concentration N_A and built-in voltage V_{bi} obtained from $C-V$ measurements.

	$N_A(\times 10^{18}\ \mathrm{cm}^{-3})$	V_{bi}(V)
$V+$ (down)	1.17	0.45
$V+$ (up)	1.04	0.74
$V-$ (down)	1.17	0.42
$V-$ (up)	1.05	0.82

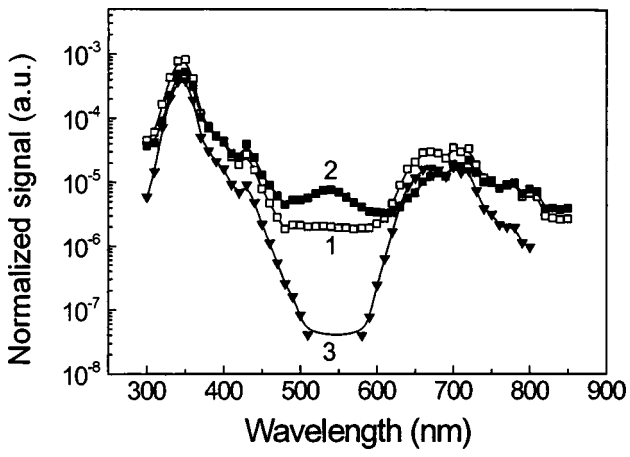

FIG. 6. Spectral distribution of the photoconductivity of a Au/PZT(65/35)/Pt structure with semitransparent top gold electrode: (1) +1 V; (2) −1 V; and (3) short circuit.

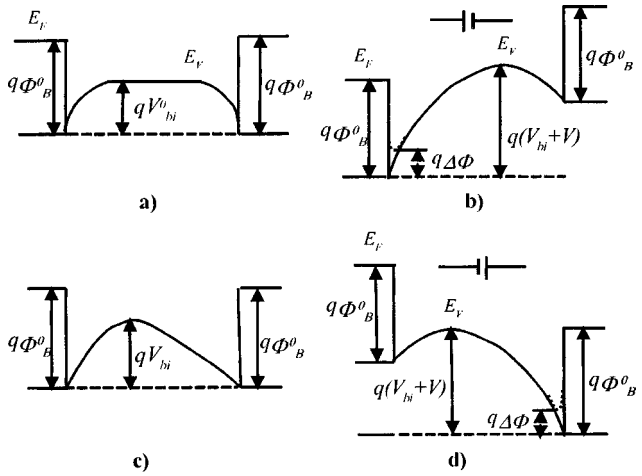

FIG. 7. Schematic band diagram of Au/*p*-PZT/Pt. (a) virgin sample (no polarization); (b) positive voltage applied; (c) zero voltage (remnant polarization); and (d) negative voltage applied. The corresponding points on the hysteresis loop are indicated in Fig. 8. The notations are usual: E_F is Fermi level; E_V is the valance band maximum; Φ_B^0 is the potential barrier at the metal-ferroelectric interface; $V_{\rm bi}^0$ is the built-in potential in a as-deposited sample; $V_{\rm bi}$ is the built-in potential in a poled sample; and $\Delta\Phi$ is the barrier lowering due to Schottky effect.

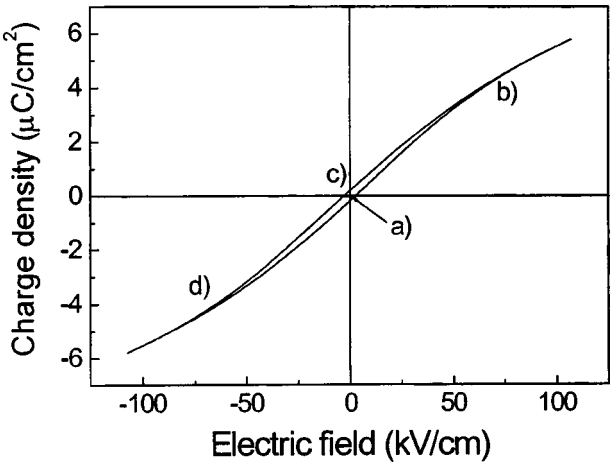

FIG. 8. $D-E$ hysteresis loop obtained by integrating the $C-V$ curve of Fig. 3 according to Eq. (2).

When the SCR is formed, only the part of the film outside this region behaves as a normal ferroelectric, meaning that polarization reversal is possible. In this case the film can be divided in two parts: one in which polarization is locked (polarization reversal is not possible due to the internal field of SCR) and one in which polarization reversal is still possible. The equivalent capacitance of the structure obtained in the (point-by-point) $C-V$ measurements is given by

$$C_{C-V} \equiv \left[C_{\rm SCR}^{-1} + C_{D-E}^{-1} \left(1 - \frac{w}{d} \right) \right]^{-1}, \tag{4}$$

where $C_{\rm SCR} = \varepsilon_0 \varepsilon_r A / w$ is the capacitance of the depletion region and w is the SCR thickness for a Schottky contact.[15] It has to be noted that, when computing $C_{\rm SCR}$, a field-independent dielectric constant was assumed, while the field-dependent dielectric constant should be considered for the capacitance of that part of the film still behaving as ferroelectric.[32] For w approaching d and/or for large values of C_{D-E} the second term in the brackets in Eq. (4) can be neglected. This means that, for a bias higher than approximately 0.6 V, the $C-V$ measurements yield essentially the capacitance of the reverse-biased contact. This justifies the use of Eq. (3) for obtaining the values presented in Table I. The finite barrier height obtained suggests the Fermi-level pinning and the existence of a depletion layer at zero bias. Due to the different metal electrodes and different annealing sequences they were subjected to, the capacitance values for two SCRs are slightly different. This asymmetry is neglected in Fig. 7, which shows how the MFM band diagram is modified when the bias is changing adiabatically.

Taking the maximum value for C_{C-V} (1.21 nF, at about 0.6 V), the C_{D-E} value at the same voltage [3.6 nF from curve (b) in Fig. 3] and considering a dielectric constant of 475, the thickness of the depletion layers can be estimated. A value of approximately 145 nm was obtained, which is about half of the film thickness (280 nm). With these numbers, the coercive field calculated from the $C-V$ curve becomes approximately 40 kV/cm, a value that is quite close to that obtained from the $D-E$ measurements. On the other hand, using the average values for N_A and $V_{\rm bi}$, the depletion layer width at the same voltage can be computed using the following formula:[19]

$$w = \sqrt{\frac{2\varepsilon_0 \varepsilon_r}{q N_A} (V + V_{\rm bi})}. \tag{5}$$

A value of about 176 nm is obtained from Eq. (5). The difference can be attributed to the influence of the interface/surface states, which was neglected in our simplified analysis of two back-to-back Schottky contacts. This influence was implicitly included in the calculation based on the measured values.

Further evidence of the fact that the ferroelectric film behaves differently when subjected to ac or dc electric fields can be obtained by integrating the $C-V$ curve. It has been claimed that, by applying this procedure, the hysteresis curve can be reconstructed.[26,33] The result of such integration is presented in Fig. 8. We remind that the charge density obtained from a $C-V$ curve ($A^{-1}\int C dV$) is not the polarization but rather the electric displacement D, according to Eqs. (1) and (2). The integration was performed considering that the entire film behaves like a normal ferroelectric, and the electric field was computed accordingly. It can be noticed that the integration produces a very small value of the charge density at $E=0$, about 0.15 μC/cm^2. The saturation value is also smaller comparing with Fig. 2. The huge difference can be explained if we consider that the polarization value depends on the amount of charge available for compensating the depolarization field. It can be assumed that in case of the $D-E$ measurements (ac electric field) the compensation is assured by the free charge from the electrodes. In the case of $C-V$ measurements (dc electric fields) it seems that the compensating charge is not enough to obtain the same value of polarization. The part of the film still behaving as a normal ferroelectric is separated from compensation charges in the metal by the SCR at least at one electrode, no matter the

voltage is positive or negative. The film is similar to a metal–ferroelectric–semiconductor structure, in which the semiconductor has the same composition as the ferroelectric. In this case the polarization value accommodates to the lowest available compensation charge that is to the charge from semiconductor. Another fact that could impede to obtain the same polarization values in the case of Fig. 2 and Fig. 8 is the opposite direction of the electric field in the SCR with respect to the applied field. To have an idea, the electric field in the SCR could be as large as 100 kV/cm, for a voltage of 1 V and using the values from Table I. Thus, the polarization in the SCR could be in the opposite direction than in the rest of the film. Moreover, there can exist a polarization gradient in the SCR due to the position-dependent field in this region.[34,35] Due to all these facts the polarization value can not be the same in $D-E$ and $C-V$ measurements. Another severe discrepancy is concerning the value of the coercive field obtained from Fig. 8. This is much smaller even than the 18.5 kV/cm estimated directly from $C-V$ measurements. The reconstruction of $P-E$ loop from the simple integration of $C-V$ curve, considering that the entire film behaves like a normal ferroelectric, can lead to wrong results when there is evidence for the presence of SCRs. However, it can be a correct procedure when the SCR influence is negligible.

B. Conductivity mechanisms

Several conduction mechanisms have been reported for MFM structures, including the field enhanced Schottky emission (SE) from the electrodes; Pool–Frenkel emission from traps (PF); Fowler–Nordheim tunneling (FN); space-charge-limited currents (SCLC), and Ohmic conductivity.[19] The latter usually occurs in low fields. For higher fields, the conduction mechanism can be controlled by interface (like SE and FN) or bulk (PF and SCLC) phenomena. The SE or FN-type conduction is strongly dependent on the electrode properties and can be considered as an electrode-controlled injection.

As it has been stated in Sec. III B, the MFM structure can be represented by two back-to-back Schottky diodes. Accordingly, the current, for any polarity, is limited by the reverse-biased diode, where the hole (rather than electron) injection from the metal occurs[36,37] into the depletion layer of the film (see Fig. 7). At a finite temperature, even for low applied voltages ($\leqslant$1 V), it is due to the thermal emission, which depends on the applied voltage because of the image force effect of lowering the barrier height (also known as Schottky emission),[19]

$$J = A^* T^2 \exp\left[-q\left(\Phi_B^0 - \sqrt{\frac{qE}{4\pi\varepsilon_0\varepsilon_d}} \right) \Big/ kT \right], \tag{6}$$

where J is the current density, A^* the Richardson constant, Φ_B^0 the barrier for the holes from the metal side, ε_d the dynamic dielectric constant of the ferroelectric film, and E the electric field at the top of the barrier, which can be estimated as

$$E = \frac{qN_A}{\varepsilon_0\varepsilon_d} w, \tag{7}$$

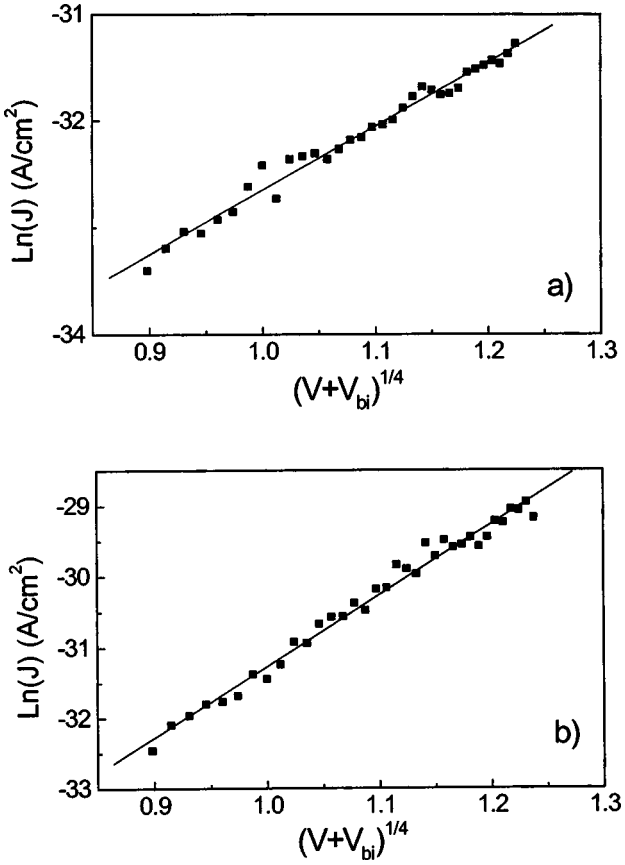

FIG. 9. Logarithmic plot of the current intensity versus $(V+V_{bi})^{1/4}$ for positive (a) and negative (b) voltages.

with w given by Eq. (5). Thus, the current–voltage characteristic is described by an expression of the form:

$$\ln J = \text{const} + b(V+V_{bi})^{1/4}, \tag{8}$$

where

$$b = \frac{q}{kT}\left(\frac{q^3 N_A}{8\pi^2\varepsilon_0^3\varepsilon_d^3} \right)^{1/4}. \tag{9}$$

The experimental $I-V$ characteristics were fitted using Eq. (8) with the values of V_{bi} and N_A obtained from the $C-V$ measurements (see Table I) and the dynamic dielectric constant was treated as adjustable parameter. The best fit, in the 0.05–1.75 V range, is presented in Fig. 9 for both positive and negative branches. It can he seen from the figure that the ''1/4 law'' (8) is obeyed, which proves that the model is qualitatively correct.

Some remarks are necessary concerning the fitted values of ε_d, which are 5.2 and 2.6 for the positive (gold electrode depletion) and negative (platinum electrode depletion) voltages, respectively. Recently, a complex model of the MFM structure was proposed, called the ''Matterhorn picture.'' [14] According to this model, there is a very thin region ($\leqslant$10 nm) near the metallic electrode, with a large concentration of trapped charge (around 10^{20} cm^{-3}) and large electric field. This layer is much thinner than the depletion SCR and is probably responsible for the pinning of the Fermi level at the metal–PZT interface. The injected carriers are strongly accelerated in this region, so, their transit time is short in com-

parison with the period of the long-wavelength optical phonon. Thus, there should be no lattice screening of the image force produced by the injected carrier, which is responsible for the barrier lowering resulting in the ''1/4 law'' (8). Consequently, ε_d appearing in Eqs. (6)–(9) is probably the optical dielectric constant ε_∞, which is equal to the squared refractive index of the material in the transparency range (in the 2.2–3.2 domain).[12–14,38] The difference in the values of the refractive index obtained from the fitting for positive and negative voltages (2.3 and 1.6, respectively) can be attributed to the different temperature of fabrication of two electrodes. While Pt electrode could interact with PZT giving rise to an interface layer with different composition, thus with different properties,[20,21] no such mixing should be expected at the Au/PZT interface.

Returning to the current–voltage characteristics, tunneling can occur at higher voltage values due to the electric field penetration in the metal electrodes.[39] Above 2 V for the positive branch and 4 V for the negative one, the current through the MFM structure began to be unstable, so, no reliable measurement was possible. This could be due to a time-dependent dielectric breakdown.

C. Photoelectric properties

The PC spectrum (Fig. 6) shows a pronounced sensitivity maximum at a wavelength of approximately 340 nm. This corresponds to the energy of 3.64 eV. The threshold wavelength (the wavelength for which the PC signal is 10% of its maximum) is approximately 370 nm, giving an energy of 3.35 eV. In a good crystalline semiconductor, this latter value should be considered as the band-gap energy, while the PC peak energy is usually determined by the balance between the number of photogenerated carriers and the rate of their surface recombination.[40] This is a smaller value compared to the band gap energy (3.75 eV) obtained in our previous paper[13] from the optical absorption spectra of similar PZT films. This discrepancy can be attributed to the presence of tails of the density of states in the gap due to the polycrystalinity of the film.[41] Our PC results imply that some of these tail states are delocalized.

There is a second broad PC maximum at about 700 nm (Fig. 6). The energy of this maximum is 1.77 eV and approximately corresponds to the half of the band-gap energy. It can be assumed that there is a quasicontinuous distribution of electronic states near the middle of the gap, which act as trapping/recombination centers. The presence of such states within the forbidden band is very plausible in polycrystalline films, and they have been observed in the absorption spectra.[13]

The presence of a short-circuit current proves the existence of an internal electric field (associated with SCR) near the top contact, where the light is absorbed. Although the shape of the spectral distribution seems to be similar, the magnitude of the photoconductive signal is dependent on the polarity of the applied voltage (compare the curves for ± 1 V). This indicates that the photocurrent is sensitive to the ferroelectric polarization orientation.

V. CONCLUDING REMARKS

We studied the electrical, ferroelectric and photoelectric properties of sol-gel derived Au–PZT65/35–Pt MFM structures. Our results allow for the following conclusions:

(i) The ferroelectric films grown by sol–gel show reasonably good ferroelectric properties, with relatively low values of the coercive field. This can be an advantage for a memory cell based on this material because of low values of the operation voltage.

(ii) The comparative analysis of the $D-E$ and $C-V$ measurement results shows that, in case of high ac fields and high frequencies, the ferroelectric properties are dominant, while in case of dc voltages the semiconductor properties of the ferroelectric film are more important. By this, we mean the formation of space charge regions near the electrodes, with the size comparable to the total thickness of the film. The presence of the SCRs does alter the effective ferroelectric properties of the film, in particular, the remnant polarization value.

(iii) The $I-V$ characteristics are consistent with the interface controlled conduction mechanisms, namely Schottky emission for intermediate voltages and possible tunneling for higher voltages. This is in agreement with the $C-V$ results showing the presence of Schottky barriers at both contacts. The results support partial depletion for our PZT65/35 film included in MFM structures.

(iv) The values obtained for the acceptor concentration, built-in potential and dynamic dielectric constant are in agreement with those reported in the literature.

(v) The studied material shows good photoelectric properties in the UV range, with a maximum sensitivity at 340 nm. This makes it interesting for UV photoconductive solid detectors.

These results imply that the interference between the semiconductor and ferroelectric properties should be carefully studied and considered when device applications of PZT-based structures are concerned. For usual semiconductor materials, a rigorous control of the growth and impurities composition is standard and indispensable for obtaining good performance devices. In the case of ferroelectric films, such a rigorous control probably has been achieved in terms of the growth but not regarding the impurities, which are unintentionally present in the film. That may lead to different results depending on the starting precursors purity, deposition technique and post-deposition annealing. Thus, our opinion is that the same technological rules as for semiconductors should be applied to ferroelectrics if good quality and reproducible devices are desired.

ACKNOWLEDGMENTS

The authors acknowledge financial support from FCT, Portugal, under Project No. POCTI/CTM/12140/1998. One of the authors (I.B.) would like thanking FCT for Grant No. PRAXIS XXI/BD/21539/99. One of the authors (L.P.) wishes to acknowledge a NATO grant, which gave him the opportunity to work at the University of Minho.

[1] J. F. Scott, L. Kammerdimer, M. Parris, S. Trayner, V. Ottenbacher, A. Shawabke, and W. F. Oliver, J. Appl. Phys. **64**, 787 (1988).
[2] M. Okuyama, Y. Matsui, H. Nakamo, and Y. Hamakawa, Ferroelectrics **33**, 235 (1981).
[3] S. Y. Wu, W. J. Takei, and M. H. Francobe, Ferroelectrics **10**, 209 (1976).
[4] G. Yi, Z. Wu, and M. Sayer, J. Appl. Phys. **64**, 2717 (1988).
[5] M. Pereira, A. G. Peixoto, and M. J. M. Gomes, J. Eur. Ceram. Soc. **21**, 1353 (2001).
[6] J. F. Scott, C. A. Araujo, B. M. Melnick, L. D. McMillan, and R. Zuleg, J. Appl. Phys. **70**, 382 (1991).
[7] N. Flouquet, J. Hector, and P. Gaucher, J. Appl. Phys. **84**, 3815 (1998).
[8] S. Thakoor and J. Maserjian, J. Vac. Sci. Technol. A **12**, 295 (1994).
[9] M. Dawber and J. F. Scott, Appl. Phys. Lett. **76**, 1060 (2000).
[10] U. Robels, J. H. Calderwood, and G. Arlt, J. Appl. Phys. **77**, 4002 (1995).
[11] M. Grossman, O. Lohse, D. Bolten, U. Boettger, T. Schneller, and R. Wasser, J. Appl. Phys. **92**, 2680 (2002).
[12] I. Boerasu, M. Pereira, M. J. M. Gomes, and M. I. C. Ferreira, J. Optoelectron. Adv. Mater. **2**, 602 (2000).
[13] I. Boerasu, M. I. Vasilevskiy, M. Pereira, M. F. Costa, and M. J. M. Gomes, Ferroelectrics **268**, 187 (2002).
[14] M. Es-Souni, A. Piorra, C.-H. Solterbeck, and M. Abed, Mater. Sci. Eng., B **86**, 237 (2001).
[15] C. M. Wang, Y. C. Chen, M. S. Lee, C. C. Chiou, and Y. T. Huang, Jpn. J. Appl. Phys., Part 1 **38**, 2831 (1999).
[16] J. Du, S. Lin, and M. Adachi, Jpn. J. Appl. Phys., Part 1 **40**, 4965 (2001).
[17] L. Pintilie and I. Pintilie, Mater. Sci. Eng., B **80**, 388 (2001).
[18] J. F. Scott, in *Advanced Microelectronics*, edited by K. Itoh and T. Sakurai (Springer, Berlin, 2000), Chap. 5–7.
[19] S. M. Sze, *Physics of Semiconductor Devices*, 2nd ed. (Wiley, 1981), Chaps. 7 and 10.
[20] S. Chung, J. W. Kim, G. H. Kim, C. O. Park, and W. J. Lee, Jpn. J. Appl. Phys., Part 1 **36**, 4386 (1997).
[21] Z. Huang, Q. Zhang, and R. W. Whatmore, J. Appl. Phys. **86**, 1662 (1999).
[22] P. Lorrain, D. R. Corson, and F. Lorrain, *Electromagnetic Fields and Waves* (Freeman, San Francisco, 1987), Chap. 9.
[23] J. Lee, C. H. Choi, B. H. Park, T. W. Noah, and J. K. Lee, Appl. Phys. Lett. **72**, 3380 (1998).
[24] M. Brazier, M. McElfresh, and S. Mansour, Appl. Phys. Lett. **72**, 1121 (1998).
[25] K. Abe, S. Komatsu, N. Yanase, K. Sano, and T. Kawakubo, Jpn. J. Appl. Phys., Part 1 **36**, 5846 (1997).
[26] R. T. Liang, Z. L. Tao, L. L. Tian, and L. Z. Jian, J. Phys. D **33**, L77 (2000).
[27] C. Shudhama, A. C. Campbell, P. D. Maniar, R. E. Jones, R. Moazzami, C. J. Mogab, and J. C. Lee, J. Appl. Phys. **75**, 1014 (1994).
[28] A. Kholkin, O. Boiarkine, and N. Setter, Appl. Phys. Lett. **72**, 130 (1998).
[29] T. Mihara and H. Watanabe, Jpn. J. Appl. Phys., Part 1 **34**, 5664 (1995).
[30] B. Nagaraj, S. Aggarwal, and R. Ramesh, J. Appl. Phys. **90**, 375 (2001).
[31] C. Hwang, B. T. Lee, C. S. Kang, K. H. Lee, H. Cho, H. Hideki, W. D. Kim, S. I. Lee, and M. Y. Lee, J. Appl. Phys. **85**, 287 (1999).
[32] F. K. Chai, J. R. Brews, R. D. Scrimpf, and D. P. Birnie III, J. Appl. Phys. **82**, 2517 (1997).
[33] K. R. Udayakumar, P. J. Schuele, J. Chen, S. B. Krupanidhi, and L. E. Cross, J. Appl. Phys. **77**, 3981 (1995).
[34] P. W. Boom, R. M. Wolf, J. F. M. Cillessen, and M. P. C. M. Krijn, Phys. Rev. Lett. **73**, 2107 (1994).
[35] Y. S. Yang, S. J. Lee, S. H. Kim, B. G. Chae, and M. S. Jang, J. Appl. Phys. **84**, 5005 (1998).
[36] B. Nagaraj, S. Aggaarwal, T. K. Song, T. Sawhney, and R. Ramesh, Phys. Rev. B **59**, 16022 (1999).
[37] I. Stolichnov and A. Tagantsev, J. Appl. Phys. **84**, 3216 (1998).
[38] M. P. Moret, M. A. C. Devillers, K. Worhoff, and P. K. Larssen, J. Appl. Phys. **92**, 468 (2002).
[39] M. Dawber, L. J. Sinnamon, J. F. Scott, and J. M. Gregg, Ferroelectrics **268**, 35 (2002).
[40] V. L. Bonch-Bruevich and S. G. Kalashnikov, *Physics of Semiconductors* (Nauka, Moscow, 1990), Chap. 7.
[41] B. Dulieu, J. Bullot, J. Wery, M. Richard, and L. Brohan, Phys. Rev. B **53**, 10641 (1996).